Modeling Thermal Contact Resistance: A Scale Analysis Approach

M. Bahrami
Research Assistant Professor,
Mem. ASME

J. R. Culham
Associate Professor,
Mem. ASME

M. M. Yovanovich
Professor,
Fellow ASME

Microelectronics Heat Transfer Laboratory,
Department of Mechanical Engineering,
University of Waterloo, Waterloo, ON,
Canada N2L 3G1

A compact analytical model is developed for predicting thermal contact resistance (TCR) of nonconforming rough contacts of bare solids in a vacuum. Instead of using probability relationships to model the size and number of microcontacts of Gaussian surfaces, a novel approach is taken by employing the "scale analysis method." It is demonstrated that the geometry of heat sources on a half-space for microcontacts is justifiable for an applicable range of contact pressure. It is shown that the surface curvature and contact pressure distribution have no effect on the effective microthermal resistance. The present model allows TCR to be predicted over the entire range of nonconforming rough contacts from conforming rough to smooth Hertzian contacts. A new nondimensional parameter, i.e., ratio of the macro- over microthermal resistances, is introduced as a criterion to identify three regions of TCR. The present model is compared to collected TCR data for SS304 and showed excellent agreement. Additionally, more than 880 experimental data points, collected by many researchers, are summarized and compared to the present model, and relatively good agreement is observed. The data cover a wide range of materials, mechanical and thermophysical properties, micro- and macrocontact geometries, and similar and dissimilar metal contacts. [DOI: 10.1115/1.1795238]

Introduction

Heat transfer through interfaces formed by mechanical contact of rough solids has many important applications, such as in microelectronics chip cooling, spacecraft structures, and nuclear fuel-temperature prediction. Heat transfer across the interface can take place by three different modes: i) conduction at the microcontacts, ii) conduction through the interstitial fluid in the gap between the contacting solids, and iii) thermal radiation across the gap. The radiation heat transfer remains small and can be neglected when surface temperatures are not too high [1]. The mean separation between contacting bodies is sufficiently large (of order micrometers) that nanoscale effects influencing radiation heat transfer can be neglected. An order-of-magnitude analysis of the controlling heat transfer modes in the gap between contacting bodies indicates that the heat flux attributed to Stefan-Boltzman radiation is small and can also be neglected.

The interstitial fluid is assumed to be absent, thus the only remaining heat transfer mode is conduction through the microcontacts. In addition, the thermal rectification is not considered in this paper. This is the phenomenon in which thermal resistance is larger in one direction than in the other due to dissimilar materials.

Engineered or real surfaces have roughness and surface curvature/out-of-flatness simultaneously. Due to surface roughness, contact between two surfaces occurs only over microscopic contacts, which are located in the ''contact plane.'' The real area of contact, i.e., the total area of microcontacts, is a small fraction of the nominal contact area, typically a few percent [2,3]. As illustrated in Fig. 1, the macrocontact area—the area where microcontacts are distributed—is formed as a result of surface curvature of contacting bodies. Heat flow is constricted to pass through the macrocontact and then microcontacts. This phenomenon is observed through a relatively high temperature drop across the interface. Here an example is given to show the magnitude and relative importance of TCR versus the ''bulk resistance.'' Consider two 3 cm^2 flat SS plates with a thickness of 5 mm and surface roughness of 1 μm. The TCR for the bare joint in a vacuum under 0.1 MPa contact pressure, is approximately 30 K/W compared to the plate bulk resistance of 0.2 K/W.

Bahrami et al. [4] reviewed the existing theoretical TCR models. They divided TCR modeling procedures into geometrical, mechanical, and thermal analyses and discussed aspects of each component of the analysis in detail. Comparing to more than 400 experimental data points, Bahrami et al. [4] showed that the existing analytical models are applicable only to the limiting cases, namely, conforming rough contacts and smooth sphere-flat contacts and do not cover the entire range of TCR. Therefore, the need for a theoretical model that can predict TCR over the entire range of contacts still exists.

The objective of this study is to develop a compact analytical model for predicting TCR over the entire range of nonconforming rough contacts, i.e., from conforming rough to smooth sphere-flat contact. A novel approach is taken by employing scale analysis methods to achieve this goal.

Theoretical Background

Analytical, experimental, and numerical models have been developed to predict TCR since the 1930s. A large number of publications on TCR exist in the literature, which shows that the development of a general predictive model is difficult, to name a few Clausing and Chao [5], Lambert and Fletcher [6], and Nishino et al. [7]. A comprehensive review of the literature can be found in Bahrami et al. [4]. In this study, only a short review of the materials used to develop the present model is given.

According to the examination of the microgeometry of rough surfaces, surface asperities have small slopes and curved shapes at their summits [8,9]. It is a common methodology to simplify the contact of two Gaussian rough surfaces by the contact of a smooth plane with a random rough surface that has equivalent surface characteristics. The equivalent surface roughness σ and surface slope m can be found from

$$\sigma = \sqrt{\sigma_1^2 + \sigma_2^2} \quad \text{and} \quad m = \sqrt{m_1^2 + m_2^2} \tag{1}$$

Cooper et al. [10] showed that the microcontacts can be assumed

Contributed by the Heat Transfer Division for publication in the JOURNAL OF HEAT TRANSFER. Manuscript received by the Heat Transfer Division October 17, 2003; revision received June 11, 2004. Associate Editor: G. Chen.

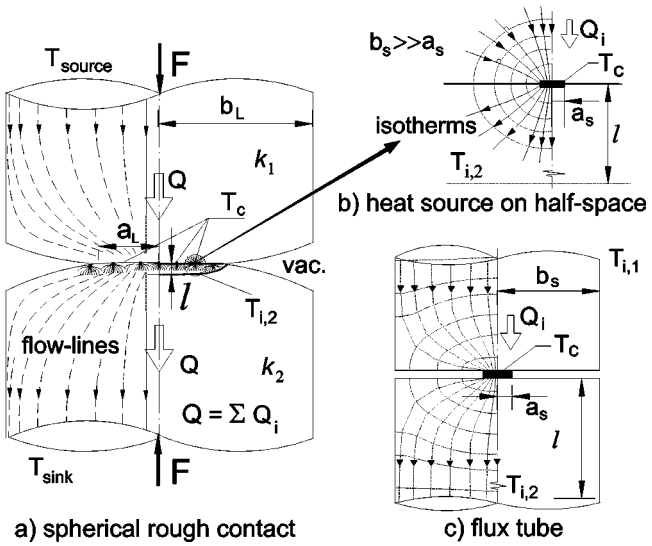

Fig. 1 Schematic geometry of spherical rough contact in vacuum, heat source on half-space, and flux tube geometries

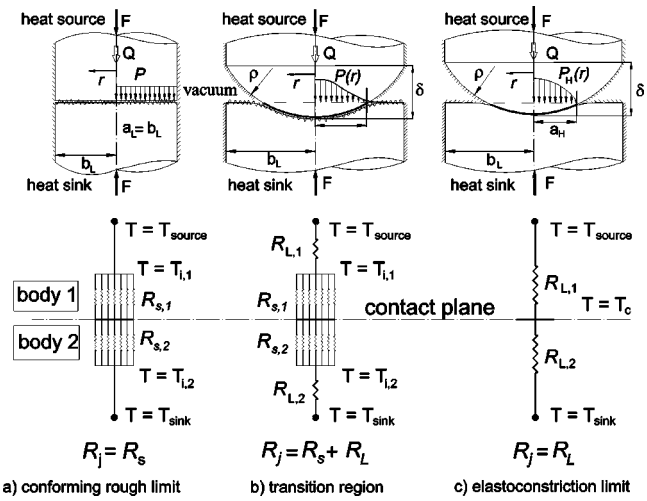

Fig. 2 Conforming rough, elastoconstriction, and transition regions

isothermal provided the thermal conductivity in each body is independent of direction, position, and temperature.

Thermal spreading resistance is defined as the difference between the average temperature of the contact area and the average temperature of the heat sink/source, divided by the total heat flow rate Q [1], i.e., $R=\Delta T/Q$. The real shapes of microcontacts can be a wide variety of singly connected areas, depending on the local profile of the contacting asperities. Yovanovich et al. [11] studied the steady-state thermal constriction resistance of a singly connected planar contact of arbitrary shape. They proposed a definition for thermal constriction resistance based on the square root of the contact area. Square root of the contact area was found to be the characteristic dimension and a nondimensional constriction resistance based on the square root of area was proposed, which varied by less than 5% for all shapes considered. Therefore, the real shape of the microcontacts would be a second-order effect, and an equivalent circular contact, which has the same area, can represent the microcontacts.

Yovanovich and Hegazy [12] showed through experiments that the surface microhardness is much higher than the bulk hardness and that the microhardness decreases as the indentation depth increases, until the bulk hardness is reached. They proposed a correlation for determining the microhardness,

$$H_{mic}=c_1(d_v/\sigma_0)^{c_2} \tag{2}$$

where d_v μm, c_1 GPa, c_2, and $\sigma_0=1$ μm are the Vickers indentation diagonal, correlation coefficients determined from the Vickers microhardness measurement, and a reference value, respectively. Microhardness depends on several parameters: roughness, mean absolute slope of asperities, method of surface preparation, and applied pressure. Sridhar and Yovanovich [13] suggested empirical relations to estimate Vickers microhardness coefficients, using the bulk hardness of the material. Two least-squares cubic fit expressions were reported

$$\begin{aligned} c_1&=H_{BGM}(4.0-5.77\kappa+4.0\kappa^2-0.61\kappa^3)\\ c_2&=-0.57+0.82\kappa-0.41\kappa^2+0.06\kappa^3 \end{aligned} \tag{3}$$

where $\kappa=H_B/H_{BGM}$, H_B is the Brinell hardness of the bulk material, and $H_{BGM}=3.178$ GPa. The above correlations are valid for the range $1.3\leqslant H_B\leqslant 7.6$ GPa; the RMS percent difference between data and calculated values was reported: 5.3% and 20.8% for c_1, and c_2, respectively. Milanez et al. [14] investigated the effect of microhardness coefficients on TCR by comparing the TCRs computed from the measured versus the estimated [from Eq. (3)] microhardness coefficients. They concluded that despite the difference between the measured and estimated values of microhardness coefficients, the TCRs predicted by both methods are in good agreement.

As shown in Fig. 1, there are two geometries that can be used as basic elements to model the thermal constriction/spreading resistance of the microcontacts, i) heat source on a half-space in which microcontacts are assumed to be located far from each other, where thermal constriction/spreading resistance of a circular microcontact of radius a_s can be found from

$$R_{mic,\text{half-space}}=\frac{1}{2k_s a_s} \tag{4}$$

where $k_s=2k_1k_2/(k_1+k_2)$, and ii) the flux tube geometry, considering the effect of neighboring microcontacts. Cooper et al. [10] proposed a simple accurate correlation for determining the flux tube constriction/spreading resistance,

$$R_{mic,\text{flux tube}}=\frac{\psi(\varepsilon_s)}{2k_s a_s} \tag{5}$$

where $\psi(\varepsilon_s)=(1-\varepsilon_s)^{1.5}$ and $\varepsilon_s=a_s/b_s$.

For smooth spherical contacts, Hertzian theory can be used to calculate the radius of the macrocontact area a_H. Hertz replaced the geometry of two spheres by a flat surface and an equivalent sphere, where the effective radius of curvature is $1/\rho=1/\rho_1+1/\rho_2$. Hertz derived a relationship for the radius of the contact area

$$\begin{aligned} a_H&=\left(\frac{3F\rho}{4E'}\right)^{1/3}\\ \frac{1}{E'}&=\frac{1-\upsilon_1^2}{E_1}+\frac{1-\upsilon_2^2}{E_2} \end{aligned} \tag{6}$$

where E, υ, and E' are the Young's modulus, Poisson ratio, and effective elastic modulus, respectively. Clausing and Chao [5] modeled the surface out-of-flatness by a spherical profile. For surfaces with large radii of curvature (approaching flat), they proposed an approximate relationship between radius of curvature and surface out-of-flatness as $\rho=b_L^2/2\delta$, where δ is the maximum out-of-flatness of the surface (see Fig. 2). Using the flux tube correlation [Eq. (5)] and neglecting the effect of surface roughness, the joint resistance for the smooth sphere-flat contact (i.e., elastoconstriction limit [15]) can be determined from

$$R_{j,\mathrm{EC}}=\frac{(1-a_H/b_L)^{1.5}}{2k_s a_H} \tag{7}$$

Comparison between the elastoconstriction model [i.e., Eq. (7)] and the smooth sphere-flat experimental data shows good agreement [4], thus the flux tube solution can be employed for determining the macrothermal resistance.

Macro- and Microthermal Resistances

As illustrated in Fig. 1, when the heat flow rate Q is transferred from a heat source at T_{source} to a heat sink at T_{sink}, it experiences the macrothermal constrictions $R_{L,1}$ and $R_{L,2}$, which arose due to the macrocontact area. Heat is then passed through n_s (parallel) microcontacts in the contact plane, which is called the effective microcontact resistance R_s. Therefore, TCR of a nonconforming rough joint in a vacuum can be written as

$$R_j=R_L+R_s \tag{8}$$

where $R_{\mathrm{L}}=R_{\mathrm{L},1}+R_{\mathrm{L},2}$, $R_{\mathrm{s}}=R_{\mathrm{s},1}+R_{\mathrm{s},2}$, and

$$\frac{1}{R_{\mathrm{s},1\ \mathrm{or}\ 2}}=\sum^{n_s}\frac{1}{R_{\mathrm{mic},1\ \mathrm{or}\ 2}}$$

where $R_{\mathrm{mic},1\ \mathrm{or}\ 2}$ is the sum of thermal constriction and spreading resistances of a single microcontact in body 1 or 2.

Equation (8) is a general expression and applicable to all spherical rough contacts; it was used by many researchers, such as Clausing and Chao [5], Nishino et al. [7], and Lambert and Fletcher [6]. A proof of Eq. (8) is given as follows. Assuming circular isothermal microcontacts, at T_c, that have a mean radius in the order of $a_s\sim\mu$m, isothermal planes must exist at intermediate temperatures $T_{i,1}$ and $T_{i,2}$ (i.e., $T_{\mathrm{source}}<T_{\mathrm{i},1}<T_c<T_{i,2}<T_{\mathrm{sink}}$) at some location l above/below the contact plane in body 1 and 2, respectively. If the microcontacts are considered as heat sources on a half-space the distance between these intermediate isothermal planes and the contact plane $l=40a_s\sim40\ \mu$m [1]. As microcontacts grow in size and number, they start to affect each other (the flux tube geometry) and l decreases, $l\sim b_s$ [16]. Consequently, macrothermal constriction/spreading resistances $R_{\mathrm{L},1}$ and $R_{L,2}$ are in series between the heat source and the isothermal plane $T_{i,1}$ and the isothermal plane $T_{\mathrm{i},2}$ and the heat sink, respectively. Also microcontacts provide n_s parallel paths for transferring heat between two isothermal planes $T_{\mathrm{i},1}$ and $T_{\mathrm{i},2}$.

Two limiting cases can be distinguished for Eq. (8): i) the conforming rough limit (i.e., contact of flat rough surfaces where the surface curvatures are very large thus macrothermal resistance R_L is negligible and microthermal resistance R_s is the controlling part), ii) the elastoconstriction limit where the radii of curvature of contacting bodies are small and surfaces are smooth, thus the macrothermal resistance R_L is predominant and R_s is negligible, and iii) transition region or general contact in which both R_L and R_s exist and have the same order of magnitude. Figure 2 shows the abovementioned regions and their corresponding thermal resistance networks. Later, a nondimensional parameter will be introduced, and a criterion will be proposed to specify these limits.

The Present Model

Due to the random nature of the surface roughness, studying the deformation and heat transfer of each single asperity is impossible; instead a representative (modeled) asperity is chosen and studied. Surface roughness is modeled by assuming a Gaussian distribution of asperities. The RMS surface roughness σ is a measure for the mean surface asperity heights.

In this section, using scale analysis, first an expression is derived for TCR of conforming rough contacts R_s. Then, the nonconforming macrocontact area is divided into infinitesimal surface elements where the conforming rough model relation can be applied. By integrating the local conductance over the macrocontact, an effective microcontact resistance R_s is found. Using the flux-tube correlation, the macrocontact resistance R_L is computed. Finally, superimposing the macro- and microthermal resistances [i.e., Eq. (8)] the joint resistance is determined.

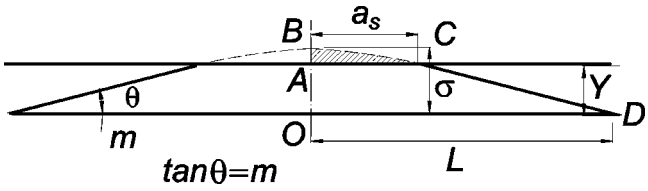

Fig. 3 Schematic geometry of microcontact

TCR of the Conforming Rough Limit. Surface roughness can be visualized as shallow valleys and hills with small slopes where asperities have spherical shapes at their summits. Figure 3 illustrates a model asperity, which represents the equivalent rough surface characteristics σ and m, placed in contact with a smooth plate at a mean separation Y. Using the equivalent rough surface simplification and considering that the mean surface slope m is small, one can assume that the microcontacts are flat and in the same contact plane. As discussed previously, the shape of microcontacts can be assumed circular. Figure 3 also illustrates a schematic geometry of a representative microcontact and proportionalities between the mean microcontact radius a_s and the surface roughness σ and slope m. In triangles ΔOBD and ΔABC, one can write $AC\propto OD$ from similar triangles. We also know that $AC=a_s$ and $OD=L=\sigma/m$, which leads to $a_s\propto\sigma/m$. This is in agreement with Kimura [17] who proposed that the ratio of roughness to asperity slope σ/m, instead of roughness itself, should be recognized as the parameter characterizing the geometrical property of the surface.

Considering n_s circular microcontacts with the mean radius of a_s within the macrocontact area, the real contact area is $A_r\propto\pi n_s a_s^2\propto\pi n_s(\sigma/m)^2$. The microcontacts are assumed to deform plastically, i.e., each microcontact can be visualized as a small microhardness indenter. The empirical correlation proposed by Yovanovich and Hegazy [12], see Eq. (2), is used to estimate the microhardness. Preserving the microcontact area (i.e., $A_v=\pi a_s^2$), where A_v is the projected area of the Vickers microhardness test, the Vickers indentation diagonal d_v can be related to the mean radius of microcontacts a_s, $d_v=\sqrt{2\pi}a_s$, microhardness becomes

$$H_{mic}\propto H^*\equiv c_1\left(\frac{\sigma}{m\sigma_0}\right)^{c_2} \tag{9}$$

Assuming plastic deformation of microcontacts, external force can be related to the real contact area and surface microhardness through a force balance,

$$F=A_r H_{mic}\propto\pi n_s\left(\frac{\sigma}{m}\right)^2 H^* \tag{10}$$

where H_{mic} is the microhardness of the softer material in contact. From Eq. (10) the number of microcontacts can be determined

$$n_s\propto\frac{F}{\pi(\sigma/m)^2 H^*} \tag{11}$$

It can be seen from Eq. (11) that an increase in load creates new microcontacts, while the mean size of microcontacts remains constant (i.e., $a_s\propto\sigma/m$). It should be noted that the size of microcontacts already in contact will increase as the load increases, or the mean separation Y decreases. However, the mean size of microcontacts, including new microcontacts generated, remains essentially constant. This is in agreement with Greenwood and Williamson [3] and also satisfies the proportionality $A_r\propto F$ reported by Tabor [2].

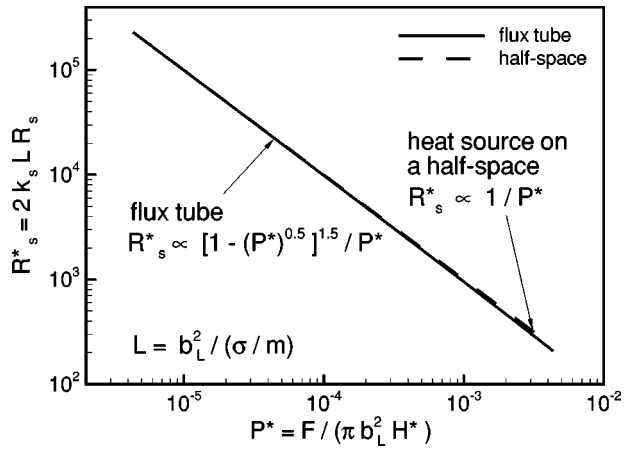

Fig. 4 Comparison between half-space and flux tube solutions

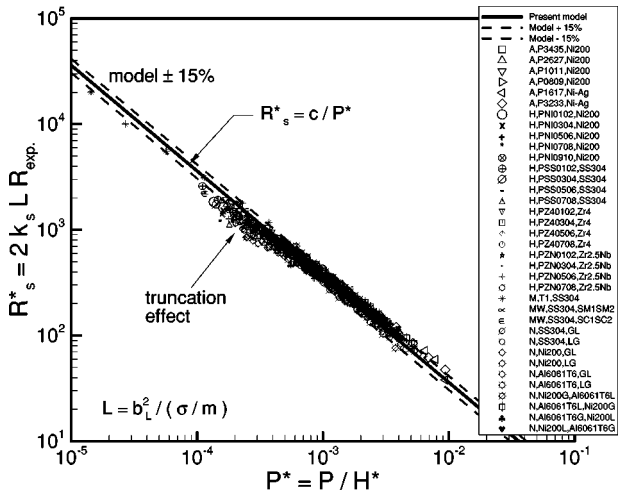

Fig. 5 Comparison between scale analysis model and data, conforming rough limit

The thermal model is based on the premise that n_s heat channels, covering the nominal contact area, form a set of parallel paths for transferring heat flow. If the half-space assumption is considered [see Fig. 1(*b*)] TCR can be found from

$$R_{s,\text{half-space}}=\frac{1}{2k_s n_s a_s}\propto\frac{1}{2k_s n_s(\sigma/m)} \tag{12}$$

Many researchers including Cooper et al. [10] modeled the microthermal constriction/spreading resistance using the flux tube geometry, thus TCR is

$$R_{s,\text{flux tube}}=\frac{\psi(\varepsilon_s)}{2k_s n_s a_s}\propto\frac{\psi(\varepsilon_s)}{2k_s n_s(\sigma/m)} \tag{13}$$

where $\psi(\cdot)$ is the constriction alleviation factor given in Eq. (5). The apparent contact area is covered by flux tubes with a mean radius b_s, and the relative size of microcontacts can be found from $\varepsilon_s=a_s/b_s=\sqrt{A_r/A_a}$, where $A_a=\pi b_L^2$. Substituting A_r and A_a one obtains

$$\varepsilon_s\propto\sqrt{\frac{F/\pi b_L^2}{H^*}}\equiv\sqrt{P^*} \tag{14}$$

where P^* is a nondimensional parameter that can be interpreted as the ratio of the nominal contact pressure to the pressure at the microcontacts. The number of microcontacts can be expressed in terms of P^* from Eq. (11)

$$n_s\propto\frac{b_L^2}{(\sigma/m)^2}P^* \tag{15}$$

We find the TCR for conforming rough surfaces by using the nondimensional parameter P^* and the flux tube solution

$$R_{s,\text{flux tube}}\propto\frac{(\sigma/m)(1-\sqrt{P^*})^{1.5}}{2k_s b_L^2 P^*} \tag{16}$$

or in the non-dimensional form

$$R^*_{s,\text{flux tube}}=2k_s L R_s\propto\frac{(1-\sqrt{P^*})^{1.5}}{P^*} \tag{17}$$

where $L=b_L^2/(\sigma/m)$ is the conforming rough limit length scale. The TCR for conforming rough surfaces, using the heat source on a half-space solution, can be found by substituting Eq. (15) into Eq. (12)

$$R^*_{s,\text{half-space}}\propto\frac{1}{P^*} \tag{18}$$

Figure 4 shows the comparison between Eqs. (17) and (18). It can be seen that over a wide range of P^*, they are almost identical and show very good agreement. However, as expected, at relatively large values of P^* the half-space relationship [Eq. (18)] shows slightly higher resistances than the flux tube. The RMS relative difference between two relationships is less than 4%. Therefore, the microcontacts can be modeled as heat sources on a half-space, and Eq. (18) is chosen for thermal analysis of microcontacts.

Using scale analysis techniques we derived Eq. (18), which illustrates that the TCR of microcontacts is inversely proportional to the dimensionless pressure (or external load). To find the equality or exact relationship, Eq. (18) must be multiplied by the scale-analysis constant c, which can be found through comparison with experimental data, i.e.,

$$R_s^*=\frac{c}{P^*} \tag{19}$$

The dimensional forms of thermal resistance and conductance using $h_s=1/(R_s A_a)$ are

$$R_s=\frac{\pi c(\sigma/m)H^*}{2k_s F}$$
$$h_s=\frac{2}{\pi c}k_s\left(\frac{m}{\sigma}\right)\frac{P}{H^*} \tag{20}$$

where c and $P=F/(\pi b_L^2)$ are the scale-analysis constant and nominal contact pressure, respectively. From Eqs. (20) and (10), it can be seen that the effective microthermal resistance is inversely proportional to the real contact area, i.e., $R_s\propto(\sigma/m)/(k_s A_r)$.

Approximately 610 experimental data points collected by Antonetti [18], Hegazy [19], Milanez et al. [20], McWaid [21], and Nho [22] are summarized, nondimensionalized, and plotted along with Eq. (19) in Fig. 5 with $c=0.36$. Minimizing the RMS difference between the model [Eq. (19)] and the experimental data, the constant of the scale analysis c was found to be $c=0.36$. The relative RMS and the mean absolute difference between the data and the relationship are 14.1% and 10.9%, respectively. Table 1 indicates the researchers and the specimen materials used in the experiments. Table 2 lists the data set number (the number that was originally assigned to the experimental data set by the researchers); the geometrical, mechanical, and average contact temperature, and the thermophysical properties of the experimental data, as reported.

Table 1 Researchers and specimen materials used in comparisons

Ref.	Researcher	Material(s)
A	Antonetti [18]	Ni 200 Ni 200-Ag
Bah	Bahrami [25]	SS 304
Blo	Bloom [28]	SS 17-4 PH
B	Burde [27]	SPS 245, CS
CC	Clausing and Chao [30]	Al 2024 T4 Brass Anaconda Mg AZ 31B SS303
CM	Cassidy and Mark [29]	SS 416
F	Fisher [31]	Ni 200-Carbon Steel
FG	Fletcher and Gyorog [32]	Brass 360 Mg Az 31B SS 304
G	Gyorog [33]	SS 304
H	Hegazy [19]	Ni 200 SS 304 Zircaloy 4 Zr-2.5%wt Nb
K	Kitscha [34]	Steel 1020-CS
MM	McMillan and Mikic [35]	SS 303
MR	Mikic and Rohsenow [16]	SS 305
M	Milanez et al. [20]	SS 304
MW	McWaid [21]	SS 304
N	Nho [22]	Al 6061 T6 Ni 200 SS 304 Ni⇆Al
SG	Smuda and Gyorog [36]	SS 304

Nho [22] studied the contact of ground with lapped surfaces. He showed that the grinding process generates near-Gaussian surface heights distributions. The surface slope was estimated from $m=\sqrt{m_{\min}m_{\max}}$, where $m_{\min}$ and $m_{\max}$ are the minimum and maximum surface slopes measured by the profilometer. Nho [22] carried out an extensive experimental program with similar and dissimilar metals (i.e., aluminum alloy 6061 T6, nickel 200, and SS 304 pairs) over a broad range of thermophysical properties and contact pressure. The [22] data are named to show the heat flow direction and the surface preparation method, for example, "N, Ni200-G, Al6061T6-L" means that the experiment was conducted between ground nickel 200 and lapped aluminum 6061 T6, and the heat flow direction was from nickel to aluminum specimen. As can be seen in Fig. 5, Nho's data show a negligible directional effect for similar metals. Additionally, the directional effect is not observed in nickel 200 and aluminum 6061 T6 pairs, but for nickel 200 and SS 304 pairs a large deviation from the predicted TCR is observed; those data are not included in the comparison.

As can be observed in Fig. 5, a common trend can be recognized in most of the conforming rough data sets. Experimental data show a lower resistance at relatively light loads compared with the model; the data approach the model as the load increases. This phenomenon, which is called the *truncation effect* [20], is important at light loads when surfaces are relatively rough. A possible explanation for this trend is the Gaussian assumption of the surface asperities, which implies that asperities with "infinite" heights exist. Milanez et al. [20] experimentally studied the truncation effect and proposed correlations for maximum asperities heights as functions of surface roughness.

Yovanovich [23] proposed an accurate correlation for determining the thermal conductance of conforming rough contacts based on the analytical model of Cooper et al. [10]

$$h_c=1.25k_s\left(\frac{m}{\sigma}\right)\left(\frac{P}{H_{mic}}\right)^{0.95} \tag{21}$$

Comparison of Eq. (20) with $[c=0.36]$ and Eq. (21) reveals that the present model and the Yovanovich [23] correlation are in good agreement over moderate and high loads, $1\times10^{-4}\leqslant P/H_{mic}\leqslant 2\times10^{-2}$; for relatively light loads, $P/H_{mic}\leqslant 1\times10^{-4}$, Eq. (20) predicts higher resistances.

General Model. Bahrami et al. [24] studied mechanical contact of spherical rough surfaces. Assuming elastic bulk deformation and plastic deformation for microcontacts, a general contact pressure distribution was proposed that covers nonconforming contacts ranging from spherical rough to smooth Hertzian contacts. A simple correlation was proposed for calculating the radius of the macrocontact as a function of two nondimensional parameters,

$$a_L=1.80a_H\frac{\sqrt{\alpha+0.31\tau^{0.056}}}{\tau^{0.028}} \tag{22}$$

where $\alpha=\sigma\rho/a_H^2$ and $\tau=\rho/a_H$ are the roughness parameter introduced by Johnson [9] and the geometric parameter, respectively.

The thermal macroresistance can be found by using the flux tube correlation [Eq. (5)] and the radius of the macrocontact area given by Eq. (22)

$$R_L=\frac{(1-a_L/b_L)^{1.5}}{2k_sa_L} \tag{23}$$

In Eq. (23), it is assumed that the radii of two contacting bodies are the same (i.e., $b_{L,1}=b_{L,2}=b_L$). In the general case where $b_{L,1}\neq b_{L,2}$, thermal spreading resistance will be $R=\psi(a/b)/4ka$.

The macrocontact area is a circle, thus the heat transferred in a nonconforming rough contact under vacuum conditions can be calculated from

$$Q=2\pi\Delta T_s\int_0^{a_L}h_s(r)rdr \tag{24}$$

where $h_s(r)$ and $\Delta T_s=T_{i,1}-T_{i,2}$ are the local thermal conductance, and the effective temperature difference for microcontacts, respectively. The effective microthermal conductance for a joint can be defined as $h_s=Q/A_a\Delta T_s$. Therefore, the effective microcontact thermal resistance, where $R=1/hA_a$ is

$$R_s=\frac{1}{2\pi}\left[\int_0^{a_L}h_s(r)rdr\right]^{-1} \tag{25}$$

Assuming constant pressure in the surface elements dr, one can calculate the local thermal conductance at r from Eq. (20)

$$h_s(r)=\frac{2}{c\pi}k_s\left(\frac{m}{\sigma}\right)\frac{P(r)}{H^*} \tag{26}$$

where $P(r)$ is the local contact pressure at r. Substituting Eq. (26) into Eq. (25), one obtains

$$R_s=\frac{cH^*(\sigma/m)}{4k_s}\left[\int_0^{a_L}P(r)rdr\right]^{-1} \tag{27}$$

From a force balance, we know that $F=2\pi\int_0^{a_L}P(r)rdr$, therefore, Eq. (27) simplifies to

$$R_s=\frac{c\pi H^*(\sigma/m)}{2k_sF} \tag{28}$$

Table 2 Summary of geometrical, mechanical and thermo-physical properties, conforming rough contacts

Reference, test # and material	E'	σ/m	c_1/c_2	k_s	b_L	$\overline{T_c}$
	GPa	μm	GPa	W/mK	mm	°C
A,P3435,Ni200	112.09	8.48/0.344	6.3/−0.26	67.1	14.3	110
A,P2627,Ni200	112.09	1.23/0.139	6.3/−0.26	64.5	14.3	150
A,P1011,Ni200	112.09	4.27/0.237	6.3/−0.26	67.7	14.3	100
A,P0809,Ni200	112.09	4.29/0.240	6.3/−0.26	67.3	14.3	108
A,P1617,Ni-Ag	63.90	4.45/0.255	0.39/0	100.0	14.3	195
A,P3233,Ni-Ag	63.90	8.03/0.349	0.39/0	100.0	14.3	190
H,PNI0102,Ni200	112.08	0.90/0.110	6.3/−0.26	75.3	12.5	120
H,PNI0304,Ni200	112.08	3.43/0.190	6.3/−0.26	76.0	12.5	115
H,PNI0506,Ni200	112.08	4.24/0.188	6.3/−0.26	75.9	12.5	110
H,PNI0708,Ni200	112.08	9.53/0.228	6.3/−0.26	75.7	12.5	115
H,PNI0910,Ni200	112.08	13.94/0.233	6.3/−0.26	75.8	12.5	115
H,PSS0102,SS304	113.74	0.48/0.072	6.3/−0.26	19.2	12.5	140
H,PSS0304,SS304	113.74	2.71/0.116	6.3/−0.26	19.1	12.5	145
H,PSS0506,SS304	113.74	5.88/0.146	6.3/−0.26	18.9	12.5	130
H,PSS0708,SS304	113.74	10.95/0.19	6.3/−0.26	18.9	12.5	125
H,PZ40102,Zircaloy4	57.26	0.61/0.049	3.32/−0.15	16.6	12.5	130
H,PZ40304,Zircaloy4	57.26	2.75/0.148	3.32/−0.15	17.5	12.5	155
H,PZ40506,Zircaloy4	57.26	3.14/0.129	3.32/−0.15	18.6	12.5	155
H,PZ40708,Zircaloy4	57.26	7.92/0.207	3.32/−0.15	18.6	12.5	160
H,PZN0102,Zr2.5Nb	57.26	0.92/0.083	5.88/−0.27	21.3	12.5	165
H,PZN0304,Zr2.5Nb	57.26	2.50/0.162	5.88/−0.27	21.2	12.5	170
H,PZN0506,Zr2.5Nb	57.26	5.99/0.184	5.88/−0.27	21.2	12.5	165
H,PZN0708,Zr2.5Nb	57.26	8.81/0.200	5.88/−0.27	21.2	12.5	160
M,T1,SS304	113.74	0.72/0.041	6.27/−0.23	18.8	12.5	39
MW,SS304,SM1SM2	113.74	1.34/0.105	4.8/0	16.0	12.7	52
MW,SS304,SC1SC2	113.74	1.44/0.089	4.5/0	16.0	12.7	52
N,SS304,GL	113.74	0.97/0.061	5.12/−0.29	19.5	12.5	175
N,SS304,LG	113.74	0.97/0.061	5.12/−0.29	19.5	12.5	185
N,Ni200,GL	112.08	0.87/0.050	4.6/−0.21	68.9	12.5	195
N,Ni200,LG	112.08	0.87/0.050	4.6/−0.21	69.4	12.5	185
N,Al6061T6,GL	39.11	0.86/0.058	0.9/−0.006	211.4	12.5	223
N,Al6061T6,LG	39.11	0.86/0.058	0.9/−0.006	211.5	12.5	227
N,Ni200-G,Al6061T6-L	56.23	0.90/0.048	1.1/−0.008	104.3	12.5	168
N,Al6061T6-L,Ni200-G	56.23	0.90/0.048	1.1/−0.008	102.7	12.5	210
N,Al6061T6-G,Ni200-L	56.23	1.20/0.057	1.03/−0.001	108.1	12.5	135
N,Ni200-L,Al6061T6-G	56.23	1.20/0.057	1.03/−0.001	108.8	12.5	125

Equations (20) and (28) are identical, which implies that the effective thermal microresistance R_s is not a function of the surface curvature. Additionally, the pressure-distribution profile does not affect the thermal microresistance. Through experiments, it can be observed that the joint resistance R_j increases as surface curvature decreases from the conforming $\rho\to\infty$ toward nonconforming contacts, if all other input contact parameters remain constant. This increase arises due to the formation of the macrocontact area and, consequently, the macroresistance R_L. It should be noted that the effective microthermal resistance R_s remains unchanged as surface curvature varies [Eq. (28)].

By superimposing the macro- and the microresistances [Eq. (8)], the thermal joint resistance for a spherical rough contact is obtained

$$R_j=\frac{0.565H^*(\sigma/m)}{k_sF}+\frac{(1-a_L/b_L)^{1.5}}{2k_sa_L} \tag{29}$$

From Eq. (29) one can conclude that i) the effective microthermal resistance, except for the thermal conductivity, is only a function of the contact microscale characteristics (i.e., surface roughness σ, slope m, microhardness H^*, and the load F), and ii) on the other hand, the macrothermal resistance is a function of the macroscale contact parameters, the macrocontact radius a_L, and size of the contacting bodies b_L. The macrocontact radius is a function of the effective elasticity modulus E', radius of curvature ρ, surface roughness σ, and the load F [Eq. (22)].

The applied load and surface roughness appear to play important roles in both macro- and microthermal resistances. The effect of surface roughness on the macroresistance is limited to the macrocontact radius a_L. The applied load is the connecting bridge between the macro- and micromechanical analyses, since the force balance must be satisfied in both analyses.

Equation (29) is a general relationship that covers both limiting cases and the transition region. It can be easily seen that in the conforming rough limit where $a_L\to b_L$, the macroresistance $R_L\to 0$, and Eq. (29) yields Eq. (20). Also, in the elastoconstriction limit where $\sigma\to 0$, the microresistance $R_s\to 0$ and $a_L\to a_H$, and Eq. (29) is reduced to Eq. (7).

Dividing both sides of Eq. (29) by R_s, one obtains

$$\frac{1.77k_sF}{H^*(\sigma/m)}R_j=1+\Theta \tag{30}$$

where Θ is the ratio of the macro- to microthermal resistances

$$\Theta=\frac{F(1-a_L/b_L)^{1.5}}{1.13H^*(\sigma/m)a_L} \tag{31}$$

Θ is a nondimensional parameter that includes the applied load, macro- and microgeometrical parameters (i.e., σ, m, ρ, and b_L) as well as the elastic and plastic mechanical properties of the contacting bodies E' and H^*. Based on this nondimensional parameter, a criterion can be defined for the elastoconstriction and conforming rough limits,

$$\begin{cases}\Theta\ll 1 & \text{conforming rough}\\ \Theta\gg 1 & \text{elastoconstriction}\end{cases} \tag{32}$$

As expected, Θ is independent of the thermal conductivity.

Equation (29) can be nondimensionalized with respect to the conforming rough limit length scale L and rewritten

$$R_j^*=2k_sLR_j=\frac{0.36}{P^*}+\frac{L(1-a_L/b_L)^{1.5}}{a_L} \tag{33}$$

where $L=b_L^2/(\sigma/m)$ and $P^*=F/(\pi b_L^2H^*)$.

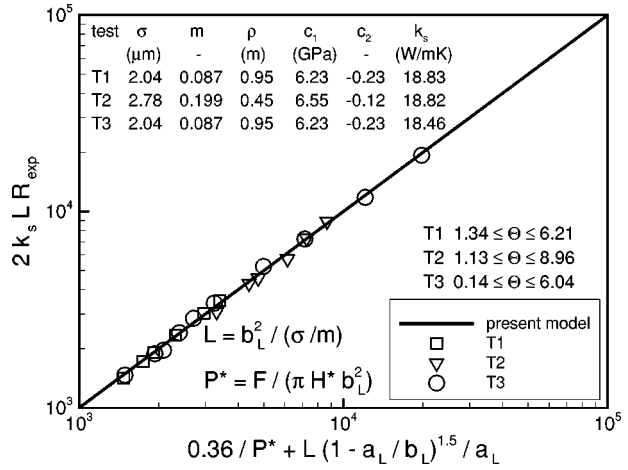

Fig. 6 Comparison between data [25] and present model

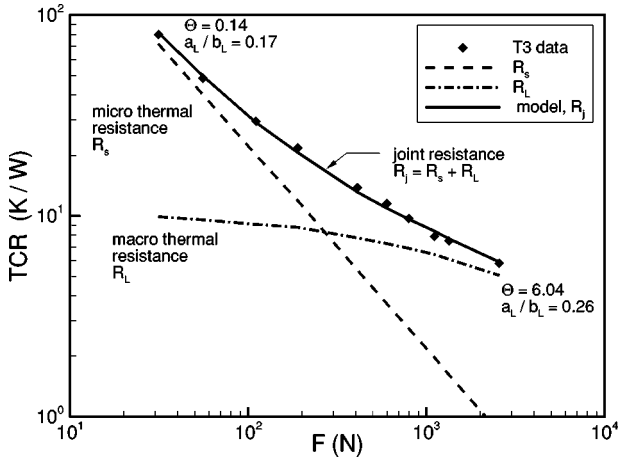

Fig. 7 Micro-, macro-, and joint thermal resistances for data set T3

Comparison With Experimental Data

To verify the general model, an experimental program was conducted to obtain data for nonconforming rough contacts in a vacuum [25]. The contact assembly included a bead-blasted flat specimen placed in contact with a smooth, polished, spherical sample in series with an ARMCO iron flux meter in a vacuum chamber. Both the flat and spherical specimens were made of SS304, $E=207$ GPa and $\nu=0.3$. Samples were machined into cylindrical shapes of 25 mm diam and 45 mm length. Both contact specimens and the flux meter were prepared for placement of six thermocouples by drilling holes that were 0.64 mm diam and 2.5 mm deep. Thermocouples were placed along the samples length so that the temperature distribution within each section could be determined. These thermocouples were located 5 mm apart with the first one 10 mm from the contact surface. The thermal conductivity of the ARMCO iron flux meter was known and used to measure the heat flow rate transferred through the contact. Also, separate tests were conducted to correlate the thermal conductivity of SS304 specimens as a function of temperature. The temperature distributions within the flat and spherical specimens were used to determine the contact temperature drop by extrapolating to the contact plane.

The flatness deviation of the flat specimens was checked using an optical flat, before bead-blasting. In general, the out-of-flatness deviation was less than 0.3 μm. The surface roughness and slope of the flat samples were measured using a Taylor-Hobson ST3 Plus Talysurf profilometer. Eight randomly selected traces of surface height profile were taken from each bead-blasted specimen. Each trace was approximately 1 cm long. The average values of surface roughness and slope are shown in Fig. 6, the RMS difference between the mean values and the measurements is approximately 6%.

Three sets of data were collected as indicated by Tests 1–3. Two radii of curvature were chosen for spherical samples, 0.45 and 0.95 m. Radii of curvature of spherical samples were measured using a Mitutoyo BHN 305 coordinate measuring machine. For each spherical sample, five separate radii of curvature were measured; the averaged values are shown in Fig. 6. The maximum relative difference between the average radii and measurements is less than 3.5%.

Mean contact temperatures of tests were recorded in the range of 45 to 145°C. The applied load was varied from 28 to 2600 N. The measured thermal joint resistance values were nondimensionalized and compared to the general model [i.e., Eq. (33)] in Fig. 6. A comprehensive uncertainty analysis based on a differential error analysis method [26] is performed in [25] to estimate the uncertainty of the collected data. The accuracy of the experimental data is approximately 5.8%. The maximum relative difference between the model and the data is 6.84%; the RMS difference between the model and data sets T1, T2, and T3 are 2.43, 4.13, and 3.84%, respectively.

The experimental program was designed to study and cover the transition region where the magnitude of the micro- and macrothermal resistances are comparable. Since a large number of reliable TCR data are available for the conforming rough and the elastoconstriction limits, no tests were conducted in these limiting regions. The values chosen for radii of curvature, load, and surface roughness provides TCR data over a relatively wide range of the transition region, $0.14\leqslant\Theta\leqslant 8.96$, see Fig. 6. To verify the reproducibility of experiments, Test 3 was conducted with the same radius of curvature and surface roughness of Test 1; new specimens were used over a wider range of applied load compared to T1. The relative importance of the micro- and macrothermal resistances is shown in Fig. 7 for the data set T3, as the applied load increases. The ratio of a_L/b_L varies from 0.17 to 0.26 as the load increases from 28 to 2561.5 N. Also the microresistance becomes smaller and the macroresistance dominates the joint resistance by increasing the load. Observe that, even at relatively large load of 2561.5 N, the radius of the macrocontact area covers only 26% of samples radius b_L. The spherical specimens have large radii of curvature, e.g. $\rho=0.95$ m, or equivalently the maximum out-of-flatness of 82 μm for T3. These samples seem flat, and

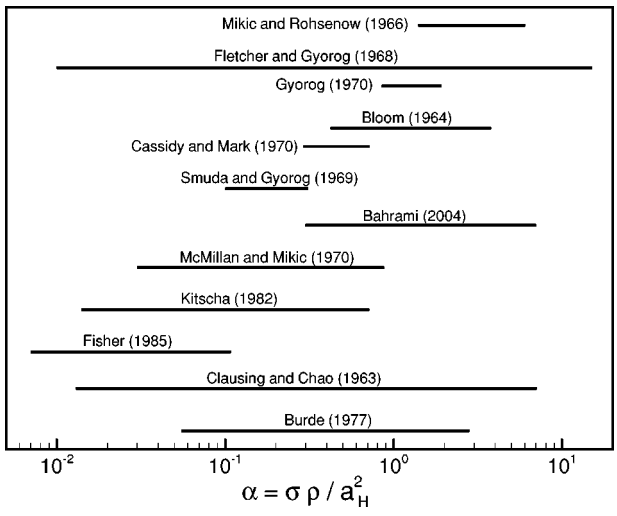

Fig. 8 Range of roughness parameter α for experimental data used in comparison

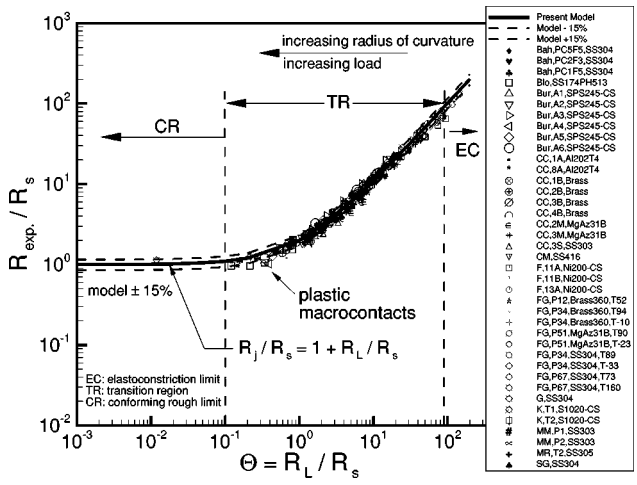

Fig. 9 Comparison between general model and nonconforming rough data

their surface curvatures cannot be detected by the naked eye, yet surface curvatures cause a relatively large thermal resistance even at high loads. This clearly shows the significance and impact of the surface curvature (out-of-flatness) on TCR.

Approximately 260 experimental data points collected by Burde [27], Bloom [28], Cassidy and Mark [29], Clausing and Chao [30], Fisher [31], Fletcher and Gyorog [32], Gyorog [33], Kitscha [34], McMillan and Mikic [35], Mikic and Rohsenow [16], and Smuda and Gyorog [36] are summarized through a comprehensive literature review. The nondimensional roughness parameter $\alpha = \sigma\rho / a_H^2$ is an important mechanical parameter for the spherical rough contacts. As the roughness parameter approaches zero the contact pressure and the macrocontact radius approaches the Hertzian values. The roughness parameter may be reduced by i) increasing the load, ii) decreasing surface roughness, and iii) decreasing the radius of curvature. Figure 8 summarizes the range of the roughness parameter for the experimental data used in the comparison. As shown, the above data sets cover a wide range of the roughness parameter.

The collected data were nondimensionalized and compared with the model [Eq. (30)] in Fig. 9. The three regions of TCR are also shown in the plot. The present model illustrates good agreement with the data; the RMS and mean absolute relative difference between the model and data are approximately 11.7% and 9.4%, respectively. Table 1 lists the researchers and the specimen materials used in the experiments. Table 3 lists the data set number (the number which was originally assigned to the experimental data set by the researchers); the geometrical, mechanical, and average contact temperature, and the thermophysical properties of the experimental data, as reported.

As the external load increases beyond the elastic limit of the contacting bodies, elastoplastic and plastic deformations may occur. The plastic macrocontact radius a_P is larger than the radius a_L (elastic) (i.e., $a_P > a_L$). Consequently, lower TCR will be measured; this trend can be clearly seen in the Fisher [31] data set ''F,11A,Ni200-CS'' (see Figs. 9 and 10).

More than 880 experimental data points (data sets used in comparisons in Figs. 5–9) are combined, nondimensionalized, and compared to the present model [Eq. (33)] in Fig. 10. The present model shows good agreement over the entire range of the comparison with the experimental data, which cover a wide range of the input parameters (see Table 4). The data include the contact between dissimilar metals, such as Ni 200-Al 6061 T6, Ni 200-Ag, and SS-CS.

Table 3 Summary of geometrical, mechanical and thermophysical properties, nonconforming contacts

Reference, test # and material	E'	σ/m	ρ	c_1/c_2	k_s	b_L	$\overline{T_c}$
	GPa	μm	m	GPa	W/mK	mm	°C
Blo,SS17,4PH,513	107.69	2.71/0.15	31.63	4.33/0	15.2	25.4	−60
Bur,A1,SPS245,CS	113.74	0.63/0.04	0.0143	3.93/0	40.7	7.15	70
Bur,A2,SPS245-CS	113.74	1.31/0.07	0.0143	3.92/0	40.7	7.15	70
Bur,A3,SPS245-CS	113.74	2.44/0.22	0.0143	3.92/0	40.7	7.15	70
Bur,A4,SPS245-CS	113.74	2.56/0.08	0.0191	4.44/0	40.7	7.15	70
Bur,A5,SPS245-CS	113.74	2.59/0.10	0.0254	4.44/0	40.7	7.15	70
Bur,A6,SPS245-CS	113.74	2.58/0.10	0.0381	4.44/0	40.7	7.15	70
CC,1A,Al2024T4	37.86	0.43/0.06	13.80	1.72/−0.04	136.8	12.7	104
CC,8A,Al2024T4	38.66	2.26/0.14	14.66	1.73/−0.04	141.4	12.7	110
CC,1B,Brass	49.62	0.47/0.06	3.87	3.02/−0.17	125.0	12.7	171
CC,2B,Brass	49.62	0.50/0.06	4.07	3.02/−0.17	125.0	12.7	129
CC,3B,Brass	51.92	0.50/0.06	3.34	3.02/−0.17	101.5	12.7	71
CC,4B,Brass	49.62	0.50/0.06	4.07	3.02/−0.17	125.0	12.7	127
CC,2M,MgAz31B	25.64	0.11/0.03	30.32	0.41/0	96.0	12.7	100
CC,3M,MgAz31B	25.64	0.11/0.03	12.41	0.41/0	96.0	12.7	100
CC,3S,SS303	113.74	0.11/0.03	21.17	4.59/−0.13	17.8	12.7	118
CM,SS416	106.04	0.126/0.08	13.44	2.62/0	24.9	12.7	
F,11A,Ni200-CS	112.62	0.12/0.04	0.0191	4.00/0	57.9	12.5	40
F,11B,Ni200-CS	112.62	0.12/0.04	0.0381	4.00/0	57.9	12.5	40
F,13A,Ni200-CS	112.62	0.06/0.03	0.0381	4.00/0	58.1	12.5	40
FG,P12,Brass360,T52	54.13	0.07/0.02	28.91	1.08/0	107.0	12.7	52
FG,P34,Brass360,T94	53.56	2.21/0.14	2.56	1.13/0	112.0	12.7	94
FG,P34,Brass360,T-10	55.84	2.21/0.14	2.56	1.13/0	98.0	12.7	−10
FG,P51,MgAz31B,T90	23.36	0.16/0.03	0.8077	0.47/0	88.0	12.7	90
FG,P51,MgAz31B,T-23	26.21	0.16/0.03	0.8077	0.62/0	70.0	12.7	−23
FG,P34,SS304,T89	106.04	1.17/0.10	9.62	2.06/0	15.9	12.7	89
FG,P34,SS304,T−33	106.04	1.17/0.10	9.62	2.85/0	13.5	12.7	−33
FG,P67,SS304,T73	106.04	0.11/0.03	0.4019	2.85/0	15.6	12.7	73
FG,P67,SS304,T160	106.04	0.11/0.03	0.4019	2.85/0	16.6	12.7	160
G,SS304	106.04	0.79/0.08	72.00	4.00/0	16.2	12.7	155
K,T1,Steel1020-CS	113.74	0.76/0.08	0.0130	4.00/0	48.0	12.7	
K,T2,Steel1020-CS	113.74	0.13/0.03	0.0130	4.00/0	51.4	12.7	
MM,P1,SS303	113.74	2.70/0.07	0.1180	4.00/0	17.3	12.7	
MM,P2,SS303	113.74	1.75/0.07	2.44	4.00/0	22.0	12.7	
MR,T2,SS305	107.14	3.87/0.21	39.69	4.2/0	19.9	12.7	
SG,SS304	106.04	0.14/0.03	70.74	4.00/0	16.2	12.7	143

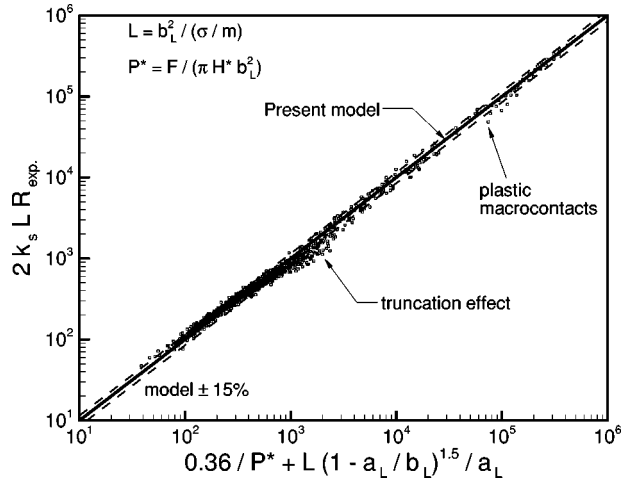

Fig. 10 Comparison of general model with all data

The surface slope m has not been reported by Clausing and Chao [30], Kitscha [34], Fisher [31], and Mikic and Rohsenow [16]. It was estimated using a correlation proposed by Lambert and Fletcher [6], $m=0.076\sigma^{0.52}$, where σ is in micrometer. Because of the abovementioned approximation to account for unreported data, the accuracy of the comparison is difficult to assess. However, the RMS and the mean absolute difference between the model and data for the entire set of data are approximately 13.8% and 10.4%, respectively. A $\pm 15\%$ bound is included in Fig. 10; 730 out of 880 data points fall into the $\pm 15\%$ bound. The accuracy of experimental data were reported by some of researchers, such as Antonetti [18], Fisher [31], and Hegazy [19], to be 8.1, 5, and 7%, respectively.

Summary and Conclusion

We show that the joint resistance is the superposition of the macro- and microthermal resistances in a vacuum. It is shown that the heat source on a half-space assumption for the geometry of microcontacts is justifiable. In other words, microcontacts are located far (enough) from each other that they do not interfere and can be considered as heat sources on a half-space. In this study, instead of using probability relationships, the scale analysis method is used and a compact TCR model is developed for the conforming rough contacts. The scale relationship satisfies the observed physical proportionality and shows the trends of the experimental data. The constant of the scale relationship is determined through comparison with experimental data. The effective microthermal resistance is observed to be inversely proportional to the real contact area and directly proportional to the surface parameter σ/m.

The scale analysis relationship derived for the conforming rough contacts is integrated over the macrocontact area to extend the scale analysis model to cover the general contact or the transition region. It is shown that the effective microthermal resistance component of the joint resistance R_s is not a function of the surface curvature/out-of-flatness. Additionally, the profile of the effective contact pressure distribution does not affect the effective microthermal resistance. The macrothermal resistance is determined using the flux tube correlation in which the radius of the macrocontact proposed by Bahrami et al. [24] is employed. Superimposing the macro- and microthermal resistances a general relationship for TCR is derived. This expression covers the entire TCR ranging from the conforming rough to the spherical smooth bare joints in a vacuum.

A new nondimensional parameter is introduced that represents the ratio of the macro- to the microthermal resistances. Based on this nondimensional parameter, a criterion is proposed for specifying the three regions of TCR (i.e., the conforming rough limit, the elastoconstriction limit, and the transition region).

Three sets of collected data for SS304 are compared to the present model, and very good agreement is observed. In addition, the present model is compared to 75 data sets, more than 880 TCR data points collected by many researchers during last 40 years that cover a wide range of surface characteristics, thermal and mechanical properties, and mean contact temperature. The RMS difference between the model and data is approximately 13.8% over the entire range of the comparison.

Table 4 Range of parameters for experimental data

Parameter
$7.15 \leqslant b_L \leqslant 14.28$ mm
$25.64 \leqslant E' \leqslant 114.0$ GPa
$7.72 \leqslant F \leqslant 16763.9$ N
$16.6 \leqslant k_s \leqslant 227.2$ W/m K
$0.04 \leqslant m \leqslant 0.34$
$0.12 \leqslant \sigma \leqslant 13.94$ μm
$-60 \leqslant \bar{T}_c \leqslant 195$ C
$0.0127 \leqslant \rho \leqslant 120$ m

Acknowledgments

The authors gratefully acknowledge the financial support of the Center for Microelectronics Assembly and Packaging (CMAP) and the Natural Sciences and Engineering Research Council of Canada (NSERC).

Nomenclature

A = area, m^2
a = radius of contact, m
b = flux tube radius, m
c = scale analysis constant
c_1 = Vickers microhardness coefficient, GPa
c_2 = Vickers microhardness coefficient
d_v = Vickers indentation diagonal, μm
dr = increment in radial direction, m
E = Young's modulus, GPa
E' = effective elastic modulus, GPa
F = external force, N
h = contact conductance, W/m^2 K
H_{mic} = microhardness, GPa
H^* = $c_1(\sigma/\sigma_0 m)^{c_2}$, GPa
k = thermal conductivity, W/m K
L = length scale$\equiv b_L^2/(\sigma/m)$, m
m = effective mean absolute surface slope
n_s = number of microcontacts
P = pressure, Pa
P^* = nondimensional pressure$\equiv F/(\pi H^* b_L^2)$
Q = heat flow rate, W
R = thermal resistance, K/W
R^* = nondimensional thermal resistance
T = temperature, K
Y = mean surface plane separation, m

Greek

α = nondimensional parameter$\equiv \sigma\rho/a_H^2$
δ = maximum surface out-of-flatness, m
ε = flux tube relative radius, a/b
θ = angle of the surface asperities, rad
Θ = nondimensional parameter$\equiv R_L/R_s$
κ = H_B/H_{BGM}
ψ = spreading resistance factor
ρ = radius of curvature, m
σ = RMS surface roughness, μm

σ_0 = roughness reference value=1 μm
τ = nondimensional parameter$\equiv\rho/a_H$
v = Poisson ratio

Subscripts

0 = value at origin
1, 2 = surface 1, 2
a = apparent
EC = elastoconstriction
H = Hertz
j = joint
L = large
mic = microcontact
P = plastic deformation
r = real
s = small, solids
v = Vickers

References

[1] Yovanovich, M. M., and Marotta, E. E., 2003, *Thermal Spreading and Contact Resistances*, chap. 4, Heat Transfer Handbook, Editors: A. Bejan and D. Kraus, Wiley, New York.
[2] Tabor, D., 1951, *The Hardness of Metals*, Oxford University Press, London.
[3] Greenwood, J. A., and Williamson, B. P., 1966, ''Contact of Nominally Flat Surfaces,'' Proc. R. Soc. London, Ser. A, **295**, pp. 300–319.
[4] Bahrami, M., Culham, J. R., Yovanovich, M. M., and Schneider, G. E., 2003, ''Review of Thermal Joint Resistance Models for Non-Conforming Rough Surfaces in a Vacuum,'' Paper No. HT2003-47051, ASME Heat Transfer Conference, Las Vegas.
[5] Clausing, A. M., and Chao, B. T., 1965, ''Thermal Contact Resistance in a Vacuum Environment,'' ASME J. Heat Transfer, **87**, pp. 243–251.
[6] Lambert, M. A., and Fletcher, L. S., 1997, ''Thermal Contact Conductance of Spherical Rough Metals,'' ASME J. Heat Transfer, **119**(4), pp. 684–690.
[7] Nishino, K., Yamashita, S., and Torii, K., 1995, ''Thermal Contact Conductance Under Low Applied Load in a Vacuum Environment,'' *Experimental Thermal and Fluid Science*, Elsevier, New York, Vol. 10, pp. 258–271.
[8] Francois, R. V., 2001, ''Statistical Analysis of Asperities on a Rough Surface,'' Wear, **249**, pp. 401–408.
[9] Johnson, K. L., 1985, *Contact Mechanics*, Cambridge University Press, Cambridge, England.
[10] Cooper, M. G., Mikic, B. B., and Yovanovich, M. M., 1969, ''Thermal Contact Conductance,'' Int. J. Heat Mass Transfer, **12**, pp. 279–300.
[11] Yovanovich, M. M., Burde, S. S., and Thompson, C. C., 1976, ''Thermal Constriction Resistance of Arbitrary Planar Contacts With Constant Flux,'' AIAA, Paper No. 76-440, Vol. 56, pp. 126–139.
[12] Yovanovich, M. M., and Hegazy, A., 1983, ''An Accurate Universal Contact Conductance Correlation for Conforming Rough Surfaces With Different Micro-Hardness Profiles,'' AIAA, Paper No. 83-1434.
[13] Sridhar, M. R., and Yovanovich, M., 1996, ''Empirical Methods to Predict Vickers Microhardness,'' Wear, **193**, pp. 91–98.
[14] Milanez, F. H., Culham, J. R., and Yovanovich, M. M., 2003, ''Comparisons Between Plastic Contact Hardness Models and Experiments,'' AIAA Paper No. 2003-0160, 41th AIAA Aerospace Meeting and Exhibit, Reno.
[15] Yovanovich, M. M., 1986, ''Recent Developments In Thermal Contact, Gap and Joint Conductance Theories and Experiment,'' ASME, Keynote Paper Delivered at 8th Int. Heat Transfer Conference, San Francisco, pp. 35–45.
[16] Mikic, B. B., and Rohsenow, W. M., 1966, ''Thermal Contact Conductance,'' Tech. Rep., Dept. of Mech. Eng. MIT, NASA Contract No. NGR 22-009-065.
[17] Kimura, Y., 1970, ''Estimation of the Number and the Mean Area of Real Contact Points on the Basis of Surface Profiles,'' Wear, **15**, pp. 47–55.
[18] Antonetti, V. W., 1983, ''On the Use of Metallic Coatings to Enhance Thermal Conductance,'' Ph.D. thesis, University of Waterloo, Dept. of Mech. Eng., Waterloo, Canada.
[19] Hegazy, A. A., 1985, ''Thermal Joint Conductance of Conforming Rough Surfaces: Effect of Surface Micro-Hardness Variation,'' Ph.D. thesis, University of Waterloo, Dept. of Mech. Eng., Waterloo, Canada.
[20] Milanez, F. H., Yovanovich, M. M., and Mantelli, M. B. H., 2003, ''Thermal Contact Conductance at Low Contact Pressures,'' J. Thermophys. Heat Transfer, **18**, pp. 37–44.
[21] McWaid, T. H., 1990, ''Thermal Contact Resistance Across Pressed Metal Contact in a Vacuum Environment,'' Ph.D. thesis, University of California Santa Barbara, Dept. of Mech. Eng.
[22] Nho, K. M., 1990, ''Experimental Investigation of Heat Flow Rate and Directional Effect on Contact Conductance of Anistropic Ground/Lapped Interfaces,'' Ph.D. thesis, University of Waterloo, Dept. of Mech. Eng., Waterloo, Canada.
[23] Yovanovich, M. M., 1982, ''Thermal Contact Correlations,'' AIAA Paper No. 81-1164, *Progress in Aeronautics and Aerodynamics: Spacecraft Radiative Transfer and Temperature Control*, T. E. Horton, ed., Vol. 83, pp. 83–95.
[24] Bahrami, M., Culham, J. R., Yovanovich, M. M., and Schneider, G. E., 2004, ''Thermal Contact Resistance of Non-Conforming Rough Surfaces, Part 1: Mechanical Model,'' J. Thermophys. Heat Transfer, **18(2)**, pp. 209–217.
[25] Bahrami, M., 2004, ''Modeling of Thermal Joint Resistance for Rough Sphere-Flat Contact in a Vacuum,'' Ph.D. thesis, University of Waterloo, Dept. of Mech. Eng., Waterloo, Canada.
[26] Holman, J. P., and Gajda, W. J., 1994, *Experimental Methods for Engineers*, McGraw-Hill, New York.
[27] Burde, S. S., 1977, *Thermal Contact Resistance Between Smooth Spheres and Rough Flats*, Ph.D. thesis, University of Waterloo, Dept. of Mech. Eng., Waterloo, Canada.
[28] Bloom, M. F., 1964, ''Thermal Contact Conductance in a Vacuum Environment,'' Douglas Aircraft Company Report SM-47700.
[29] Cassidy, J. F., and Mark, H., 1970, ''Thermal Contact Resistance Measurements at Ambient Pressure of One Atmosphere to 3×10 E-12 mm Hg and Comparison With Theoretical Predictions,'' *Progress in Aeronautics-Themophysics: Applications to Thermal Design Aircraft*, J. T. Bevans, ed., Vol. 23, pp. 23–37.
[30] Clausing, A. M., and Chao, B. T., 1963, ''Thermal Contact Resistance in a Vacuum Environment,'' Tech. Report, University of Illinois, Urbana, Report ME-TN-242-1.
[31] Fisher, N. F., 1987, ''Thermal Constriction Resistance of Sphere/Layered Flat Contacts: Theory and Experiment,'' Master's thesis, University of Waterloo, Dept. of Mech. Eng., Waterloo, Canada.
[32] Fletcher, L. S., and Gyorog, D. A., 1970, ''Heat Transfer Between Surfaces in Contact; An Analytical and Experimental Study of Thermal Contact Resistance of Metallic Interfaces,'' AIAA, Paper No. 70-852.
[33] Gyorog, D. A., 1970, ''Investigation of Thermal Isolation Materials for Contacting Surfaces,'' AIAA 8th. Aerospace Science Meeting, New York.
[34] Kitscha, W., 1982, ''Thermal Resistance of the Sphere-Flat Contact,'' Master's thesis, University of Waterloo, Dept. of Mech. Eng., Waterloo, Canada.
[35] McMillan, R., and Mikic, B. B., 1970, ''Thermal Contact Resistance With Non-Uniform Interface Pressures,'' Tech. Report, Dept. of Mech. Eng. MIT, NASA Contract No. NGR 22-009-(477).
[36] Smuda, P. A., and Gyorog, D. A., 1969, ''Thermal Isolation With Low-Conductance Interstitial Materials Under Compressive Loads,'' AIAA, Paper No. 69-25, AIAA 7th Aerospace Science Meeting, New York.